

(20). This difference is about 10% at 120 GPa and about 5% at 200 GPa. However, CsI shows no sharp volume changes, and it is difficult to expect substantial diffusion of the atoms to reconstruct the lattice to the clusters of Cs or I. If this disproportionation really exists, it has to be small, because it was observed only after laser heating at high pressures (18) and was not observed in experiments at room temperature. However, properties of the above discussed substances are not well known in this unexplored pressure region. Therefore, additional experiments are needed to exclude these other effects.

Calculations of the critical temperature of superconductivity in the hcp phase of CsI give $T_c = 0.04$ K (11). However, many uncertain parameters are involved in these calculations, and further theoretical studies are needed. In particular, it would be interesting to calculate the pressure dependence of T_c . We found that the maximum value of T_c is in the vicinity of the phase transition

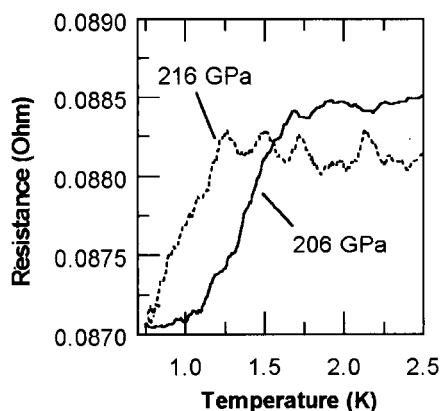


Fig. 4. Pressure dependence of the superconductive transition in CsI shown for 206 and 216 GPa. The plot at 216 GPa was obtained with a two-probe method with $R = 3.1315$ ohms at 2 K. It was shifted in the resistance scale to facilitate comparison with the plot for 206 GPa, which was obtained with the four-probe method.

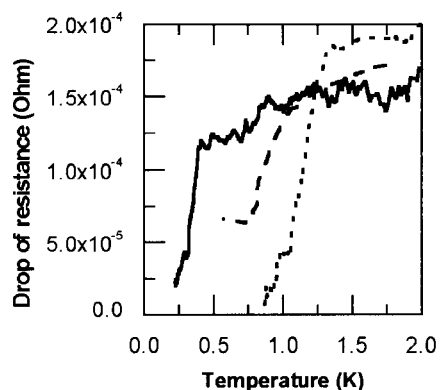


Fig. 5. Temperature dependence of resistance of CsI at 206 GPa taken at different magnetic fields: solid line, 0.5 T; dashed line, 0.07 T; and dotted line, 0 T.

to the hcp phase and that T_c decreases with increasing pressure. This finding is consistent with the pressure dependence of T_c near the phase transitions observed for other superconductors.

References and Notes

1. H. K. Mao and P. M. Bell, *Science* **200**, 1145 (1978); J. A. Xu, H. K. Mao, P. M. Bell, *ibid.* **232**, 1404 (1986); A. L. Ruoff, H. Xia, Y. Vohra, *Rev. Sci. Instrum.* **61**, 3830 (1990).
2. H. K. Mao and R. J. Hemley, *Rev. Mod. Phys.* **66**, 671 (1994), and references therein; N. W. Ashcroft, *Phys. Rev. B* **41**, 10963 (1990); C. F. Richardson and N. W. Ashcroft, *Phys. Rev. Lett.* **78**, 118 (1997).
3. S. T. Weir, A. C. Mitchell, W. J. Nellis, *Phys. Rev. Lett.* **76**, 1860 (1996).
4. S. Block and G. Piermarini, *Phys. Today* **29**, 44 (1976); H. K. Mao and P. M. Bell, in *High Pressure Research, Application in Geophysics*, M. H. Manghani and S. Akimoto, Eds. (Academic Press, New York, 1977), pp. 493–502; J. van Straaten and I. F. Silvera, *Rev. Sci. Instrum.* **58**, 994 (1987).
5. K. Shimizu, K. Amaya, S. Endo, in *High Pressure Science and Technology*, W. A. Trzeciakowski, Ed. (World, Singapore, 1996), pp. 498–500; K. Amaya et al., *Rev. High Pressure Sci. Technol.* **7**, 688 (1998); M. I. Eremets, K. Amaya, K. Shimizu, T. C. Kobayashi, *ibid.*, p. 469.
6. K. Shimizu, K. Suhara, M. Ikumo, M. I. Eremets, K. Amaya, *Nature* **393**, 767 (1998).
7. M. I. Eremets, in *Proceedings of the Adriatico Research Conference: Simple Systems at High Pressures and Temperatures: Theory and Experiment* [online], International Centre for Theoretical Physics, Trieste, Italy, 1997 (available at www.ictp.trieste.it/~pub_off/sci-abs/smr999); S. Kometani, M. Eremets, K. Shimizu, M. Kobayashi, K. Amaya *J. Phys. Soc. Jpn.* **66**, 818 (1997).
8. H. K. Mao et al., *Science* **246**, 649 (1989); H. K. Mao et al., *Phys. Rev. Lett.* **64**, 1749 (1990).
9. K. Asaumi, *Phys. Rev. B* **29**, 1118 (1984); T.-L. Huang and A. L. Ruoff, *ibid.*, p. 112; E. Knittle and R. Jeanloz, *Science* **223**, 53 (1984); *J. Phys. Chem. Solids* **46**, 1179 (1985).
10. J. Aidun, M. S. Bukowski, M. Ross, *Phys. Rev. B* **29**, 2611 (1984); S. Satpathy, N. E. Christensen, O. Jepsen, *ibid.* **32**, 6793 (1985).
11. R. Asokamani, G. Subramoniam, M. Amirthakuman, in *Recent Trends in High Pressure Research*, A. K. Singh, Ed. (Oxford Univ. Press, Oxford, 1992), pp. 434–436.
12. Q. Williams and R. Jeanloz, *Phys. Rev. Lett.* **56**, 163 (1986); I. N. Makarenko, A. F. Goncharov, S. M. Stishov, *Phys. Rev. B* **29**, 6018 (1984). Extrapolation of the pressure dependence of the optical-absorption edge gives an estimate for the onset of the metallization near 100 GPa.
13. R. Reichlin, M. Ross, S. Martin, K. A. Goettel, *Phys. Rev. Lett.* **56**, 2858 (1986). An increase of the infrared reflectivity was found at 110 GPa, which was attributed to metallization.
14. M. I. Eremets, *High Pressure Experimental Methods* (Oxford Univ. Press, Oxford, 1996), pp. 59 and 210.
15. J. H. Eggert, F. Moshary, W. J. Evans, K. A. Goettel, I. F. Silvera, *Phys. Rev. B* **44**, 7202 (1991).
16. H. K. Mao, J. Xu, P. M. Bell, *J. Geophys. Res.* **91**, 4673 (1986); R. J. Hemley, C. S. Zha, A. P. Jephcoat, H. K. Mao, L. W. Finger, *Phys. Rev. B* **39**, 11820 (1989).
17. I. F. Silvera and R. J. Wijngaarden, *Rev. Sci. Instrum.* **56**, 121 (1985).
18. Q. Williams and R. Jeanloz, *Phys. Rev. Lett.* **59**, 1132 (1987).
19. K. Takemura, unpublished data.
20. R. Reichlin et al., *Phys. Rev. B* **49**, 3725 (1994).
21. We thank K. Syassen for his critical reading of the manuscript, discussions, and valuable comments and K. Takemura for providing the state equation data for Cs before publication. This work was supported by Core Research for Evolutional Science and Technology and a grant-in-aid from Center of Excellence research (10CE20004), Japan.

20 May 1998; accepted 10 July 1998

Response of Flexible Polymers to a Sudden Elongational Flow

Douglas E. Smith and Steven Chu*

Individual polymers at thermal equilibrium were exposed to an elongational flow producing a high strain rate, and their dynamics were recorded with video fluorescence microscopy. The flow was turned on suddenly so that the entire evolution of molecular conformation could be observed without initial perturbations. The rate of stretching of individual molecules is highly variable and depends on the molecular conformation that develops during stretching. This variability is due to a dependence of the dynamics on the initial, random equilibrium conformation of the polymer coil. The increasing appearance at high strain rates of slowly unraveling hairpin folds is an example of nonergodic dynamics, which can occur when a statistical mechanical system is subjected to nonadiabatic, or "sudden," external forces.

The theoretical study of the dynamics of flexible polymer molecules in fluid flows has been an active area of research for more than 60 years, starting with the work of W. Kuhn

Departments of Physics and Applied Physics, Varian Building, Stanford University, Stanford, CA 94305, USA.

*To whom correspondence should be addressed. E-mail: schu@leland.stanford.edu

in 1934 (1). It is also an area of practical interest because dilute polymer solutions exhibit many interesting non-Newtonian rheological properties such as viscosity enhancement and turbulent drag reduction (2). Classic experiments on the dynamics of polymers in elongational flow have measured averaged quantities such as light scattering (3), birefringence (4), and rheological stress (5). These results have been compared with many

theoretical models, which are often complex enough to require analysis by computer simulation (6–9). Previously, we directly observed the stretching of a flexible polymer in elongational flow (10), and we discovered that many features of the dynamics could not be obtained from measurements of averaged quantities alone. In particular, we observed a strong heterogeneity in the dynamics and conformations of individual chains.

In earlier work (10), we observed molecules flowing continuously into a crossed-channel flow cell. Although this approach allowed us to collect data continuously, it exposed the molecules to velocity gradients (namely, a “shearing” Poiseuille flow in the inlet channels, as well as elongational flow) before the molecules entered the region where they were to be imaged. These conditions led to concerns, as noted by de Gennes (11), that the polymer might not actually be at thermal equilibrium before the inception of the elongational flow and that this preparation might cause the observed heterogeneity in the dynamics. However, the maximum flow rate was kept at half the rate that would cause measurable predeformation due to shear, as discussed [in reference 24 of (10)]. However, with the previous technique, we were limited to fluid strain rates of only about three times the natural relaxation rate of the polymer, and because of the geometry of the flow cell, we were unable to see the continuous evolution of polymer

conformation from the inception of flow.

In the present study, we overcame these limitations by suddenly turning on the flow with the polymer coils starting at rest and by using a higher viscosity solvent. These improvements allowed us to make observations at a fluid stretching rate up to 55 times as high as the polymer relaxation rate (16 times as high as the relaxation rate in the earlier study), to follow the entire dynamics from the inception of the flow, and to characterize the changes in the distribution of molecular conformations with strain rate.

A polymer in elongational flow begins to deform when the force due to hydrodynamic friction across the molecule exceeds the entropic elasticity that tends to coil it. There are two natural time scales. The first time scale is the longest relaxation time of the polymer ($\tau_{\text{polymer}} \equiv \tau$), which is the characteristic time that is necessary for Brownian motion to globally rearrange the polymer’s conformation. This relaxation time is also approximately the time that is necessary for a chain that is fully stretched by an external force to recoil back to equilibrium (12). The second time scale ($1/\dot{\epsilon}$) is set by the strain rate ($\dot{\epsilon} \equiv d\epsilon/dt$) of the applied flow, where t is time and $\epsilon \equiv \dot{\epsilon}t$ is the applied strain. The strain rate is a velocity gradient ($\partial v_x/\partial y = \dot{\epsilon}$) along the direction y of flow. Dimensional analysis suggests that the onset of polymer stretching should occur when $De \equiv \dot{\epsilon}\tau \approx 1$; the dimensionless parameter De is the Deborah number. The simple analysis is roughly correct because we found that a coil-stretch transition occurred at $De = \dot{\epsilon}\tau \approx 0.4$ (10), which is close to the more rigorous theoretical prediction of $De \approx 0.5$ (8).

A quasi-planar hyperbolic flow was produced over an $\sim 500 \mu\text{m}$ by $500 \mu\text{m}$ area in a $200\text{-}\mu\text{m}$ -deep, $650\text{-}\mu\text{m}$ -wide, crossed-channel flow cell. The cell was microfabricated from silicon as described previously (10) and gave rise to a constant velocity gradient (along an axis that is parallel to the exit channels) over an $\sim 100 \mu\text{m}$ by $100 \mu\text{m}$ imaging region. Individual molecules of fluorescently labeled lambda bacteriophage DNA (λ -DNA) (13) were imaged (14) at a depth of $\sim 100 \mu\text{m}$. These DNA molecules may be considered to be “flexible” polymers because they contain ~ 440 persistence lengths. Each molecule started at equilibrium (as a random coil) in the imaging region. To maximize the residence time of molecules, we selected molecules that closely approached the stagnation point (where the velocity goes to zero). Molecules could be positioned near the stagnation point by slight heating of one of the four tubes (two inlets and two outlets) leading to the crossed channel. To ensure that molecules were at equilibrium, we waited ~ 10 relaxation times before the flow was turned on.

The flow was turned on in less than one-thirtieth of a second (as determined by video recordings of tracer beads) by using a T valve to route pressurized fluid from a shunt tube into the flow (Fig. 1A). Images of the stretching polymers were recorded by a VCR and digitized. For the highest strain rates, individual deinterlaced video fields (one-sixtieth of a second each) were analyzed. A computer-generated cursor was used to measure the maximum extension of a molecule along the stretching axis (15), and the transient conformation of each molecule during stretching was categorized according to the types shown in Fig. 1B. (These classifications are somewhat of an oversimplification; we actually observed a continuous spectrum of different shapes.) To reach a high De value, the flow rate was increased until the images began to blur. To increase the De value further, we increased the viscosity of the solvent (a solution of sucrose and glucose) so as to increase the polymer relaxation time (13, 16). For $De = 27, 48, \text{ and } 55$, the viscosity was increased to ~ 180 centipoise (cP). The experiment was repeated many times to obtain an ensemble of molecular stretching paths.

Measurements were made at $De = 2.0, 3.4, 13.8, 27, 48, \text{ and } 55$. The first two values were chosen to match the highest De value in our previous study (10). The data for $De = 2.0$ are shown in Fig. 2A. Although the previous study could only observe molecules that had already accumulated $\epsilon = \dot{\epsilon}t = 2.5$ units of strain (which corresponds to an $\exp(2.5)$, or an ~ 12 -fold, deformation of the fluid element), the new data match the previous data over the range that could be covered previously, indicating that the heterogeneity in the dynamics and the different molecular conformations that were seen earlier were not artifacts of predeformations. By reversing the flow, we were also able to study the stretching of the same molecule repeatedly under identical conditions, allowing it to relax completely before turning on the flow again. The molecule stretched at a different rate each time and could adopt all of the various conformations that were seen in the larger ensemble of molecules. Thus, the appearance of different conformations was not a property of particular molecules but was due to a dependence of the dynamics on the initial, random equilibrium conformation of the coil.

This study reached a higher De value than did the earlier work, which was limited to $De \leq 3.4$. In Fig. 2B, dynamics in a flow of $De = 48$ are shown. Many more molecules became kinked or folded at this higher value of De . On average, folded molecules stretched the slowest, whereas kinked ones stretched the fastest. Dumbbell and half-dumbbell molecules also stretched relatively fast. The percentage of molecules assuming various conformations as a function of De is

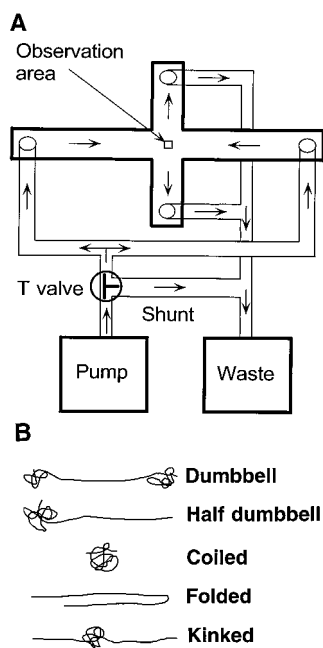


Fig. 1. (A) Schematic diagram of the apparatus. A T valve is used to turn on the flow (represented by arrows) suddenly while molecules in the region of elongational flow are observed. (B) Schematic drawings of the different transient polymer conformations observed during stretching.

presented in Fig. 3. For $De < 0.4$, there was no stretching, and all of the molecules were coils. The fractions of folded and kinked molecules increased rapidly and appeared to reach asymptotic values of about one-third for $De > 10$. Meanwhile, the fraction of dumbbell or half-dumbbell molecules increased very sharply to more than two-thirds for $De \cong 1$ and then dropped to an asymptotic value of about one-third for $De > 10$. We emphasize that these classifications (for $De > 2$) were of transient conformations during stretching, made after the molecule had experienced ≥ 2.3 units of strain [which corresponds to an $\exp(2.3)$, or an ~ 10 -fold, deformation]. The asymptotic steady-state conformation of chains in these experiments was a nearly fully stretched straight line (the steady-state extension was $>75\%$ of full contour length for $De > 2$).

Kinked, dumbbell, and half-dumbbell molecules stretch faster than folded molecules because they proceed by unraveling a near-equilibrium coiled portion of the chain, whereas a symmetrically folded molecule is in a metastable state where the drag forces on either side nearly cancel each other. Kinked, dumbbell, and half-dumbbell, molecules stretch at a similar rate, despite their different shapes, because the hydrodynamic drag across the molecule is similar whether the

ends are coiled or straightened. The drag coefficient of a $10\text{-}\mu\text{m}$ -long stretched (and hence free-draining) section of DNA is only $\sim 20\%$ greater than the drag on a nondraining, $10\text{-}\mu\text{m}$ -long coiled section (17). This result is

consistent with our observation that kinked molecules stretch only slightly faster than dumbbell-shaped ones.

We can compare the polymer's rate of stretching to the rate of deformation of the

Fig. 3. The fraction of the total ensemble of stretching molecules that develop various conformations as a function of De . These assignments were made only for molecules that experienced at least $\varepsilon = 2.3$ units of strain, which represents an $\exp(2.3)$, or an ~ 10 -fold, stretching of the fluid element. Below $De \cong 0.4$, there is no stretching and all of the molecules are coils (10). For $De > 0.4$, some molecules persist as coils, even after 2.3 units of strain, but this fraction drops to almost zero for $De > 10$. The percentages of dumbbell and half-dumbbell molecules were grouped together because there is a continuous range of molecular conformations between these categories consisting of dumbbells molecules having a smaller "bell" on one end and a larger "bell" on the other end. Molecules that were folded or kinked but also had a coiled portion at one end were classified as folded or kinked and not as half dumbbells. For a molecule to be classified as folded, we required that more than two-fifths of the total chain length was taken up in the folded portion. We also kept track of the fraction of molecules that had larger folds, in which more than two-thirds of the total chain length was taken up. The dashed line marks the fraction of molecules that are expected to have a random equilibrium configuration that would predispose them to developing into a folded shape under affine deformation (as discussed in the text and illustrated in Fig. 5).

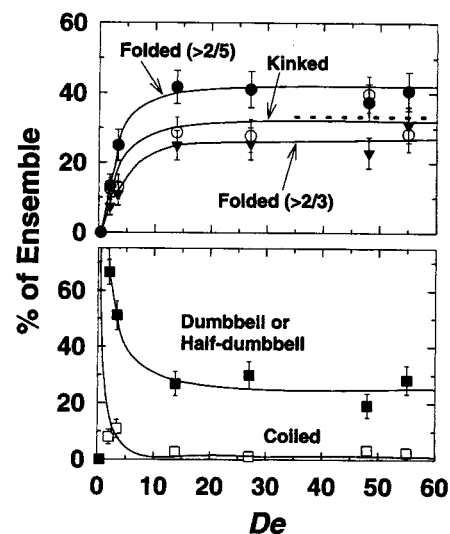
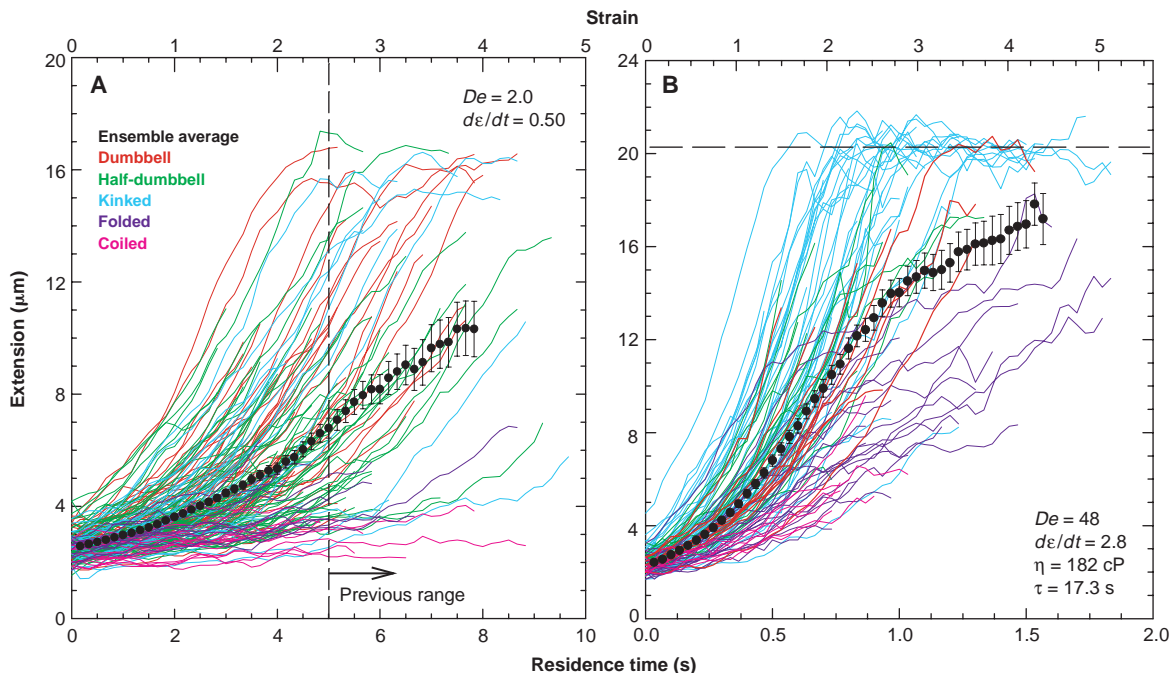


Fig. 2. (A) Extension versus residence time (or strain) for ~ 200 fluorescently labeled λ -DNA molecules (with a total contour length of $22\ \mu\text{m}$) starting at thermal equilibrium (as random coils) and stretching in a relatively weak elongational flow. Here, $De = \dot{\varepsilon}\tau = 2.0$, meaning that the fluid element is being stretched at a rate that is twice the natural relaxation rate of the polymer (about four times the critical rate for deformation). The strain rate was $d\varepsilon/dt = 0.5$, the solvent viscosity was $\eta = 43.3$ cP, and the polymer relaxation time was $\tau = 4.1$ s. The molecular conformation during stretching was categorized into one of five shapes (schematically illustrated in Fig. 1B), as indicated by the colors of the solid lines. At this relatively low De value, the dumbbell and the half-dumbbell shapes were the most prevalent. The solid black points represent the ensemble average over all of the molecules, and the vertical dashed line indicates the point below which continuous data could not be collected in an earlier version of this experiment because of the onset of measurable deformation from preshearing in the inlets (10). Suddenly turning on the flow allows data to be continuously collected from the inception of the velocity gradient. **(B)** Extension versus residence time (or strain) for



~ 120 fluorescently labeled λ -DNA molecules in a strong elongational flow ($De = 48$). The strain rate was $d\varepsilon/dt = 2.8$, the viscosity was $\eta = 182$ cP, and the relaxation time was $\tau = 17.3$ s. At this De value, there are fewer dumbbell and half-dumbbell shapes and many more folded and kinked shapes than at $De = 2.0$. On average, the folded molecules stretched slower than the other forms, whereas the kinked molecules stretched the fastest. The solid black points represent the ensemble average, and the horizontal dashed line indicates the $\sim 20.5\text{-}\mu\text{m}$ asymptotic, steady-state value of the extension, which is close to the contour length of $\sim 22\ \mu\text{m}$.

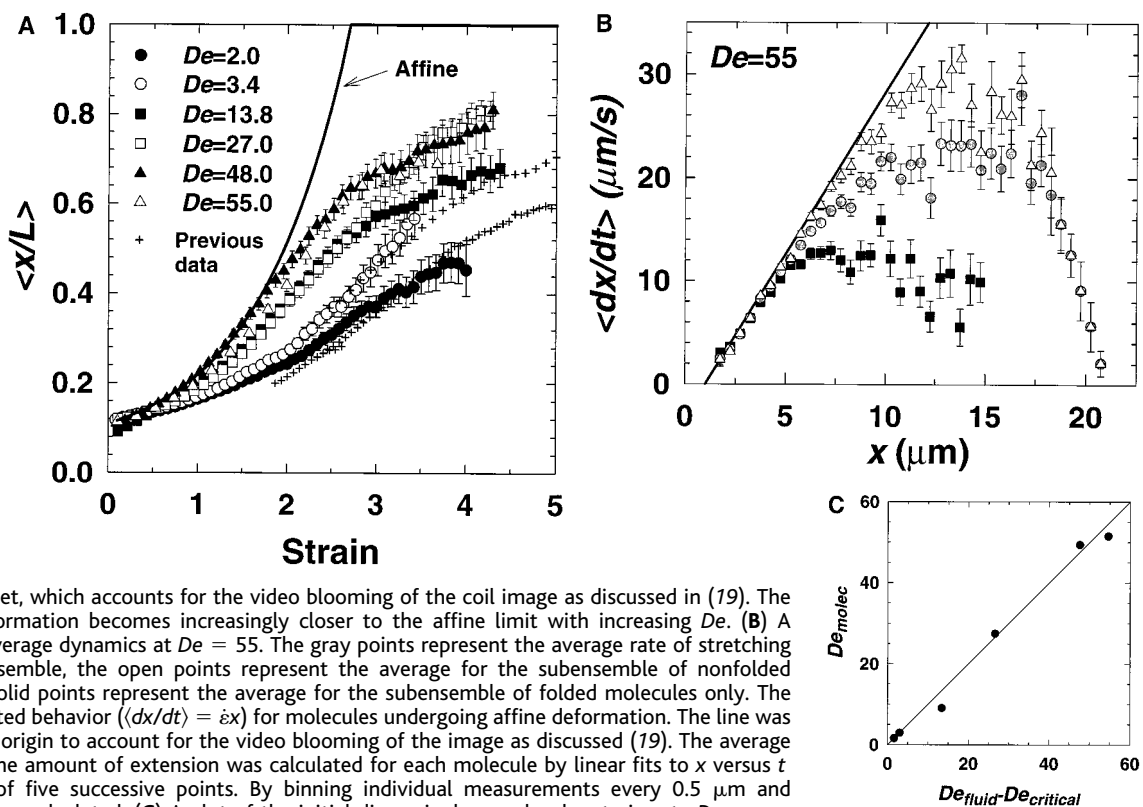
fluid element. In this flow, the fluid element is stretched exponentially in time along one axis (the elongational axis) and compressed along the other, which means that the separation of two fluid points [initially spaced at a distance $x(0)$] will increase with time t as $x(t) = x(0)\exp(\dot{\epsilon}t)$, where $\dot{\epsilon}$ is the strain rate and $\dot{\epsilon}t \equiv \epsilon$ is the accumulated fluid strain. One might expect that, for $De \gg 1$, the polymer stretching rate dx/dt would approach the fluid stretching rate because the hydrodynamic force should greatly exceed the polymer's elastic restoring force. Mathematically speaking, this case where the polymer stretches exactly with the fluid is called "affine deformation." However, a true affine deformation is not physically possible because there must be some motion of the fluid relative to the polymer ("slippage") in order for hydrodynamic drag to exert a stretching force. Also, the polymer's finite extensibility (18) inherently leads to nonaffine behavior at large extensions. The minimum amount of slippage needed to stretch the molecule occurs at the critical strain rate $\dot{\epsilon}_c \equiv 0.4/\tau$, where the coil-stretch transition appears (10). We use the term "quasi-affine deformation" to describe a deformation where the polymer begins to stretch affinely after the threshold condition $\dot{\epsilon} \geq \dot{\epsilon}_c$ is met. At that point, we might expect the observed

initial molecular strain rate $(\partial/\partial x)(dx/dt)$ to be equal to $\dot{\epsilon} - \dot{\epsilon}_c$. In the limit $De = \dot{\epsilon}\tau \gg \dot{\epsilon}_c\tau \approx 0.4$, stretching approaches true affine deformation.

The average fractional extension as a function of strain is plotted for the De range (Fig. 4A). These quantities are presented in dimensionless (or "natural") units to allow the direct comparison of data that were collected with flows of differing viscosity and strain rate. Our previous measurements at $De = 2.0$ and 3.4 are also presented for comparison. The relatively close correspondence between the average values in the old and new measurements also indicates that there was no substantial effect of the slight preshearing in the previous data. After correcting for the $\sim 1\text{-}\mu\text{m}$ overestimate of the extension due to video blooming (19), the data show that the initial $\sim 25\%$ of the deformation becomes close to the affine deformation limit for the largest value of De ($= 55$). The near overlap of the average data at early times for $De = 13.8$ and 27.0 , even after the rescaling of the axes to dimensionless units, may be due to collecting these two data sets at different solvent viscosities (45.4 and 175 cP, respectively). The high concentrations of sugar (~ 47 and 64% by mass) used to obtain these viscosities may have altered the solvent quality (the strength of solvent-solute interactions).

The stretching dynamics is conveniently analyzed by making a "phase-space" plot of the average rate of extension versus the amount of extension, as shown in Fig. 4B for $De = 55$. After accounting for the $\sim 1\text{-}\mu\text{m}$ overestimate in the measured coil size due to blooming (19) (which leads to the positive x intercept of $\sim 1\text{ }\mu\text{m}$), the initial $\sim 25\%$ of the stretching is nearly affine because it is linear and has a slope of $\dot{\epsilon}_{\text{molec}} \equiv \dot{\epsilon} - \dot{\epsilon}_c \approx \dot{\epsilon}$ (Fig. 4B). For extensions beyond $\sim 25\%$, the deformation becomes highly nonaffine because of the appearance of hairpin folds and the nonlinear elasticity. The initial affine behavior does not depend very strongly on the conformation that the polymer later develops because the subensemble of molecules that later became folded also stretched nearly affinely, although only for about the first ~ 15 to 20% of full extension, after which the development of folds begins to slow the stretching. In contrast, the subensemble of molecules that did not become folded stretch affinely up to almost 35% of full extension. The data also show that the initial extension along the stretching axis influences the resulting conformation; the initial extension of molecules that fold was slightly smaller ($2.3\text{ }\mu\text{m}$) than that of nonfolding molecules ($2.6\text{ }\mu\text{m}$). The rate of stretching of nonfolding molecules was roughly

Fig. 4. (A) The average fractional extension (extension divided by total contour length) versus strain for De values ranging from 2.0 to 55, as indicated in the legend. Crosses represent the previous data (10) at $De = 2.0$ and 3.4 in which there was a small amount of preshearing [$(dv/dt)\tau \leq 0.5$] of the polymers in the inlet channel. The solid line shows the expected behavior for affine deformation, namely, the function $x(t) = x(0)\exp(\dot{\epsilon}t) + x_{\text{offset}}$, where $x(0) = 2R_G = 1.4\text{ }\mu\text{m}$ is the average initial coil size (two times the radius of gyration R_G) and $x_{\text{offset}} = 1\text{ }\mu\text{m}$ is a constant offset, which accounts for the video blooming of the coil image as discussed in (19). The initial portion of the deformation becomes increasingly closer to the affine limit with increasing De . (B) A phase-space plot of the average dynamics at $De = 55$. The gray points represent the average rate of stretching $\langle dx/dt \rangle$ for the whole ensemble, the open points represent the average for the subensemble of nonfolded molecules only, and the solid points represent the average for the subensemble of folded molecules only. The solid line shows the expected behavior ($\langle dx/dt \rangle = \dot{\epsilon}x$) for molecules undergoing affine deformation. The line was shifted by $1\text{ }\mu\text{m}$ from the origin to account for the video blooming of the image as discussed in (19). The average rate of extension versus the amount of extension was calculated for each molecule by linear fits to x versus t over a running window of five successive points. By binning individual measurements every $0.5\text{ }\mu\text{m}$ and averaging them, $\langle dx/dt \rangle$ was calculated. (C) A plot of the initial dimensionless molecular strain rate $De_{\text{molec}} = (\partial/\partial x)(dx/dt)\tau$ (obtained from the slope of the linear portion of the phase-space plot above) versus the dimensionless fluid strain rate ($De_{\text{fluid}} = De$) (minus the critical value $De_{\text{critical}} \approx 0.4$ at the stretch-coil transition). The solid line (a slope of one) indicates the quasi-affine limit where $De_{\text{molec}} = De - De_{\text{critical}} \approx De - 0.4$. The initial stretching is almost truly affine ($De_{\text{molec}} \approx De$) for a large De value.



proportional to their initial extension.

The initial rate of stretching is, to a fairly good approximation, quasi-affine for De values ranging from 2.0 to 55 (Fig. 4C). In an earlier study, where we were not able to see the early part of the deformation for many molecules, we concluded that there was an increasing deviation (due to the appearance of folded molecules) from affine deformation as the strain rate was increased (10). By observing the initial part of the elongation, we have now refined this observation and find that there is an increasing tendency toward affine deformation with increasing De during the initial ~25% of the extension, followed by an

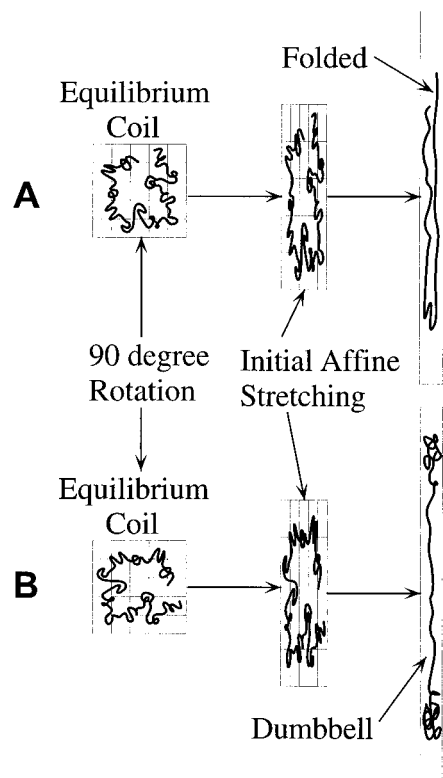


Fig. 5. A schematic diagram of the polymer deformation. The initial configuration is a random coil. (A) If the chain ends are both on the same side of the center of mass with respect to a plane perpendicular to the stretching axis (about a one-third probability for a random coil), a large fold will likely develop if the initial deformation is affine. If De is large, the suddenly elongated molecule can effectively become trapped in a folded state that is a nearly affine projection of the initial configuration. Then, because of the nonlinear elasticity, the stretching becomes slower (nonaffine) as the fold is unraveled. (B) If the same conformation is rotated by 90° so that the ends are on opposite sides of the center of mass, a dumbbell, half-dumbbell, or kinked shape will likely develop. These nonfolded shapes stretch more efficiently because they proceed from the unraveling of coiled sections of the chain, although the stretching rate is still ultimately limited by the nonlinear elasticity as the extension approaches the total contour length.

increasingly strong departure from affine deformation at larger extensions because of folds. This behavior is consistent with the predictions of some computer simulations based on a “kink dynamics” model (9, 20).

Our observations enable us to make a qualitative sketch of how the stretching leads to the appearance of different conformations (Fig. 5). If a coiled chain starts out at equilibrium with both of its ends on the same side of the center of mass with respect to a plane perpendicular to the stretching axis, a large fold is likely to develop (Fig. 5A). If the De value is large, the suddenly elongated molecule can effectively become trapped in a folded state that is a nearly affine projection of the initial configuration. A statistical analysis of the conformations of a large ensemble of random coils shows that the probability of this occurring is about one-third. This result agrees fairly well with our observation that, in the limit $De \gg 1$, ~27% of the molecules develop folds in which more than two-thirds of their contour length is taken up and ~42% of the molecules develop folds in which more than two-fifths of their contour length is taken up. However, if the same initial coil in Fig. 5A is rotated by 90° (as in Fig. 5B), it is likely to develop a dumbbell, a half-dumbbell, or kinked shape instead of a folded shape. These conformations are similar to some of those seen in computer simulations (7, 9). The results of Brownian dynamics simulations are also comparable to our results and are especially useful because they allow a detailed study of the relative roles of the initial conformation and the Brownian motion in determining the stretching pathway (21).

Finally, a few comments about the applicability of equilibrium statistical mechanics to this problem should be made. A flexible polymer's elasticity, or tendency to form a random coil, is entirely entropic in origin; there are many more accessible states of a coiled chain than of a stretched one (22). However, for $De \gg 1$, the molecule is stretched at a rate exceeding its natural relaxation rate. This process leads to a nonadiabatic change of state, during which the molecule cannot visit, through Brownian fluctuations, an appreciable fraction of the phase space of accessible conformational states. The molecule may follow a pathway to the final state that would not have occurred if the elongational flow had been turned on slowly. For example, a molecule with a hairpin fold is a metastable nonequilibrium conformation, which would clearly not occur if the elongational flow was increased adiabatically (that is, slowly, in comparison with the polymer's relaxation time). Thus, we have a situation where the dynamics are retarded relative to the situation predicted by a naive application of equilibrium statistical mechanics. This effect must be accounted for in theoretical treatments of the dynamics (23). Other examples of nonergodic behavior have been recently reported in the

femtosecond optical excitation of molecules (24) and have been conjectured to occur in protein folding scenarios (25). Nonequilibrium statistical mechanics may also play a role in the behavior of large proteins when a local driving mechanism is faster than the relaxation times between different subunits of the protein.

References and Notes

- W. Kuhn, *Kolloid Z.* **68**, 2 (1934).
- R. G. Larson, *Constitutive Equations for Polymer Melts and Solutions* (Butterworths, New York, 1988); J. D. Ferry, *Viscoelastic Properties of Polymers* (Wiley, New York, ed. 3, 1980); R. B. Bird, C. F. Curtiss, R. C. Armstrong, O. Hassager, *Dynamics of Polymeric Liquids* (Wiley, New York, 1987), vol. 2.
- K. A. Smith et al., *Colloq. Int. CNRS* **233**, 341 (1975); J. L. Lumley, *Phys. Fluids* **20**, s64 (1977); M. J. Menasveta and D. A. Hoagland, *Macromolecules* **24**, 3427 (1991).
- A. Keller and J. A. Odell, *Colloid. Polym. Sci.* **263**, 181 (1985); A. J. Muller, J. A. Odell, A. Keller, *J. Non-Newtonian Fluid Mech.* **30**, 99 (1988); G. G. Fuller and L. G. Leal, *Rheol. Acta* **19**, 580 (1980); C. A. Cathey and G. G. Fuller, *J. Non-Newtonian Fluid Mech.* **34**, 63 (1990); P. N. Dunlap and L. G. Leal, *ibid.* **23**, 5 (1987); K. A. Narh, J. A. Odell, A. Keller, *J. Polym. Sci. Polym. Phys. Ed.* **30**, 335 (1992); E. D. T. Atkins and M. A. Taylor, *Biopolymers* **32**, 911 (1992); J. A. Odell and M. A. Taylor, *ibid.* **34**, 1483 (1994); T. Q. Nguyen, G. Yu, H.-H. Kausch, *Macromolecules* **28**, 4851 (1995); N. Sasaki et al., *J. Appl. Polym. Sci.* **59**, 1389 (1996); D. Hunkeler, T. Q. Nguyen, H. H. Kausch, *Polymer* **37**, 4257 (1996); *ibid.*, p. 4271; S. Carrington and J. Odell, *J. Non-Newtonian Fluid Mech.* **67**, 269 (1996); S. Carrington et al., *Polymer* **38**, 4151 (1997); S. Carrington et al., *ibid.*, p. 4595.
- H. R. Reese and B. H. Zimm, *J. Chem. Phys.* **92**, 2650 (1990); V. Tiratmadja and T. Sridhar, *J. Rheol.* **37**, 1081 (1993); D. F. James and T. Sridhar, *ibid.* **39**, 713 (1995); S. L. Ng, R. P. Mun, D. V. Boger, D. F. James, *J. Non-Newtonian Fluid Mech.* **65**, 291 (1996); N. V. Orr and T. Sridhar, *ibid.* **67**, 77 (1996); S. H. Spiegelberg and G. H. McKinley, *ibid.*, p. 49.
- P. G. de Gennes, *J. Chem. Phys.* **60**, 5030 (1974); E. J. Hinch, *Proceedings of the Symposium on Polymer Lubrication*, Brest, France (1974); D. H. King and D. F. James, *J. Chem. Phys.* **78**, 4749 (1983); F. S. Henyey et al., *ibid.* **82**, 4362 (1985); X. Fan and R. Bird, *J. Non-Newtonian Fluid Mech.* **18**, 255 (1985); Y. Rabin et al., *J. Chem. Phys.* **85**, 4696 (1986); Y. Rabin, *ibid.* **88**, 4014 (1988); L. E. Wedgwood et al., *J. Non-Newtonian Fluid Mech.* **40**, 119 (1991); A. E. Chavez et al., *J. Stat. Phys.* **62**, 1255 (1991); J. M. Kobe et al., *J. Rheol.* **37**, 947 (1993); E. J. Hinch, *J. Non-Newtonian Fluid Mech.* **54**, 209 (1994); R. Keunings et al., *ibid.* **68**, 85 (1997); J. M. Rallison, *ibid.*, p. 61.
- D. Acerno et al., *J. Polym. Sci.* **12**, 2177 (1974); G. Ryskin, *J. Fluid Mech.* **178**, 423 (1987); J. M. Rallison and E. J. Hinch, *J. Non-Newtonian Fluid Mech.* **29**, 37 (1988); J. M. Wiest et al., *J. Chem. Phys.* **90**, 587 (1989); T. W. Liu, *ibid.*, p. 5826; P. S. Doyle, E. S. G. Shaqfeh, A. P. Gast, *J. Fluid Mech.* **334**, 251 (1997).
- R. G. Larson and J. J. Magda, *Macromolecules* **22**, 3004 (1989).
- R. G. Larson, *Rheol. Acta* **29**, 371 (1990).
- T. T. Perkins, D. E. Smith, S. Chu, *Science* **276**, 2016 (1997).
- P. G. de Gennes, *ibid.*, p. 1999.
- T. T. Perkins, S. R. Quake, D. E. Smith, S. Chu, *ibid.* **264**, 822 (1994).
- We stained the λ -DNA (Gibco BRL, Gaithersburg, MD) with YOYO-1 (Molecular Probes, Eugene, OR) at a dye:base pair ratio of 1:4 for >1 hour. The persistence length of native DNA is ~53 nm (18). When stained, the contour length increases by up to ~35% (to ~22 μ m for λ -DNA) [T. T. Perkins, D. E. Smith, R. G. Larson, S. Chu, *Science* **268**, 83 (1995)]. Experiments were performed in a pH 8 buffer consisting of 10 mM tris-HCl, 2 mM EDTA, 10 mM NaCl, 4% β -mercaptoethanol, glucose oxidase (~50 μ g/ml), and catalase (~10 μ g/ml) [10

to 18% (w/w) glucose and 40 to 55% (w/w) sucrose]. The viscosity of each solution was measured with a viscometer and was adjusted by varying the sugar concentrations. The experiments were performed at room temperature (~23°C).

14. We used a Nikon $\times 60$, 1.2 numerical aperture water immersion objective, a Zeiss 60-mm-to-infinity-corrected conversion lens, a $\times 0.25$ Zeiss tube lens, a Hamamatsu microchannel plate intensifier, and a Phillips video camera.
15. The extension data were smoothed by Gaussian weighted averages of adjacent frames.
16. We determined the relaxation time to be 3.9 s in a 41-cP sugar solution by observing the relaxation of stretched molecules as described previously (10). The relaxation time in the sugar solutions of other viscosities was assumed to be proportional to the ratio of the viscosities.
17. R. Larson, T. Perkins, D. Smith, S. Chu, *Phys. Rev. E* **55**, 1794 (1997).
18. S. B. Smith, L. Finzi, C. Bustamante, *Science* **258**, 1122 (1992); C. Bustamante, J. F. Marko, E. D. Siggia, S. Smith, *ibid.* **265**, 1599 (1994).
19. The average extension observed at zero residence time is about 2.5 μm (Fig. 2). The observed coil size appears larger than the known size of about 1.4 μm (twice the radius of gyration) because of a blooming effect in the intensified video camera when objects of saturating brightness were imaged [D. E. Smith, T. T. Perkins, S. Chu, *Macromolecules* **29**, 1372 (1996); *Phys. Rev. Lett.* **75**, 4146 (1995)]. The same effect was noted previously [S. B. Smith, P. K. Aldridge, J. B. Callis, *Science* **243**, 203 (1989)] and must be kept in mind when analyzing the data.
20. E. Hinch, *J. Non-Newtonian Fluid Mech.* **34**, 181 (1994).
21. R. Larson, in preparation.
22. See, for example, P. Flory, *Statistical Mechanics of Chain Molecules* (Interscience, New York, 1969).

23. See R. G. Winkler, P. Reineker, M. Schreiber, *Europhys. Lett.* **8**, 493 (1989) for an attempt to calculate the entropic elastic forces dynamically. However, this model does not consider the dynamics in flow or allow for features such as folds.
24. E. W.-G. Diau, J. L. Herek, Z. H. Kim, A. H. Zewail, *Science* **279**, 847 (1998).
25. J. N. Onuchic, Z. Luthey-Schulten, P. G. Wolynes, *Annu. Rev. Phys. Chem.* **48**, 539 (1997).
26. We acknowledge assistance from H. Babcock, W. Fann, R. Larson, T. Perkins, and W. Volkmuth. This work was supported in part by the U.S. Air Force Office of Scientific Research, National Science Foundation (NSF), the Human Frontiers Foundation, and by an endowment established by Theodore and Frances Geballe. D.E.S. was supported by a fellowship from the NSF Program in Mathematics and Molecular Biology.

28 May 1998; accepted 23 July 1998

Three-Dimensional Deformation Measured in an Alaskan Glacier

Joel T. Harper, Neil F. Humphrey, W. Tad Pfeffer

Measurements of movement along 28 boreholes reveal the three-dimensional flow field in a 6 million cubic meter reach of Worthington Glacier, a temperate valley glacier located in Alaska. Sliding at the bed accounted for 60 to 70 percent of the glacier's surface motion. Strain rates in the ice were low from the surface to a depth of about 120 meters, but then increased rapidly toward the bed. Ice deformation was not affected by temporal changes in the sliding rate. The three-dimensional pattern of motion indicates that plane strain, which is often assumed by models, is a poor approximation of this viscous flow.

All models for glacier motion, whether their purpose is to calculate a timeline for an ice core or to test the stability of the West Antarctic Ice Sheet, must call on various assumptions about the relations between the stresses acting on the ice body and the flow field that results. Yet, many of these relations have not been well documented with observation or laboratory measurements (1). For example, the surface velocity of glaciers can change over hours, days, or seasons—sometimes affecting the entire glacier and other times only small reaches (2). While nonsteady sliding processes at the bed are typically cited as an explanation for this variability (3), little is known about the spatial and temporal structure of internal deformation of glaciers and ice sheets. We thus measured the three-dimensional flow field within a large reach of Worthington Glacier, a temperate valley glacier located in the Chugach Mountains, Alaska (Fig. 1). Instruments were arranged on the reach—which has a volume of $6.2 \times 10^6 \text{ m}^3$ and extends 230 m in length, 150 m in width, and 180 to 200 m in depth—to image the glacier's short-term three-dimensional velocity

field. The spacing of the measurement points in all three dimensions was much less (<10%) than the ice thickness. These data offer a means for understanding the details of deformation and sliding processes.

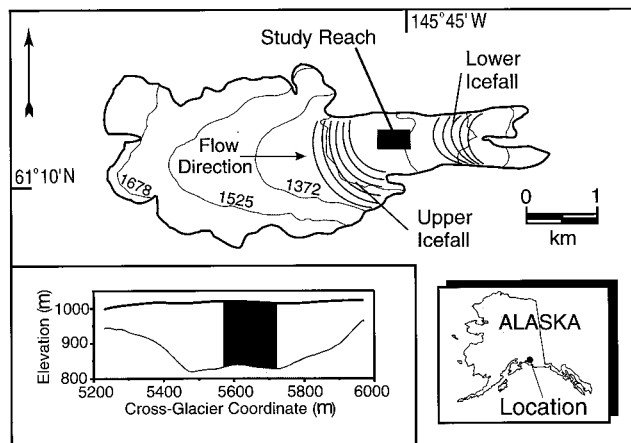
The measured reach is just below the dividing line between the accumulation and ablation areas of the glacier. Radio-echo sounding measurements indicate that the area surrounding the study reach has steep valley walls, a relatively flat valley floor, and a maximum thickness of just over 200 m (4). Located about 200 m up-glacier and 300 m down-glacier from the

reach are two icefalls, each of which drops more than 300 m vertically and is extensively crevassed. The average surface slope is 2° to 3° in the study reach, closer to 10° when averaged along the length of the glacier, and 20° to 25° through the icefalls.

The velocity field was determined by measuring the displacement over time of a network of surface markers and a vertical array of points along 28 boreholes drilled to depths of 180 to 200 m. The boreholes were drilled with a hot water system using instrumentation and methods designed to create straight holes with uniform and smooth walls. The holes were inspected for smoothness with a video camera (5) and were not fitted with casing. Most holes were drilled to about 10 m above the glacier bed so that no connection was made with the basal hydrologic system, which would have altered the drainage system and thermally eroded the holes. The boreholes were repeatedly measured with an inclinometer that quantifies both tilt and azimuth orientation of points along the hole, thus giving its full three-dimensional trajectory.

The boreholes were spaced about 20 m apart along the glacier and 30 m apart across the glacier. Data were collected at 2-m vertical intervals in each borehole. Markers and borehole trajectories were surveyed four separate

Fig. 1. The location of Worthington Glacier and the study reach. Inset in lower left shows a cross-sectional profile of the glacier extending through the study reach; the lower line is bed, the upper line is the ice surface, and the dark block is the study reach.



J. T. Harper and N. F. Humphrey, Department of Geology and Geophysics, University of Wyoming, Laramie, WY 82071, USA. W. T. Pfeffer, Institute of Arctic and Alpine Research, University of Colorado, Boulder, CO 80309, USA.